Experimental Evidence for Dark Excitons in Monolayer WSe₂

Xiao-Xiao Zhang,[1] Yumeng You,[1,2] Shu Yang Frank Zhao,[3] and Tony F. Heinz[4,5,*]

[1]*Departments of Physics and Electrical Engineering, Columbia University, 538 West 120th Street,*
New York, New York 10027, USA
[2]*Ordered Matter Science Research Center, Southeast University, Nanjing 211189, China*
[3]*Department of Physics, Harvard University, Cambridge, Massachusetts 02138, USA*
[4]*Department of Applied Physics, Stanford University, Stanford, California 94305, USA*
[5]*SLAC National Accelerator Laboratory, 2575 Sand Hill Road, Menlo Park, California 94025, USA*

Transition metal dichalcogenides in the class MX_2 (M = Mo, W; X = S, Se) have been identified as direct-gap semiconductors in the monolayer limit. Here, we examine light emission of monolayer WSe₂ using temperature-dependent photoluminescence and time-resolved photoluminescence spectroscopy. We present experimental evidence for the existence of an optically forbidden dark state of the band-gap exciton that lies tens of meV below the optically bright state. The presence of the dark state is manifest in the strong quenching of light emission observed at reduced temperatures. The experimental findings are consistent with theoretical predictions of spin-polarized conduction and valence bands at the K point of the Brillouin zone, with the minimum gap occurring between bands of opposite electron spin.

Atomically thin transition metal dichalcogenide (TMDC) crystals have recently attracted great attention because of their distinctive electronic and optical properties. Materials in the family of MX_2 (M = Mo, W; X = S, Se) have been a focus of particular interest because these layered van der Waals semiconductors undergo a transition from an indirect to a direct gap at monolayer thickness and consequently offer the possibility of efficient light emission [1,2]. These materials also exhibit unusually strong Coulomb interactions as a consequence of their two-dimensional (2D) nature and the associated reduction in dielectric screening. This gives rise to anomalously large excitonic effects, with tightly bound excitons at room temperature [3–7] and the existence of stable higher-order excitonic complexes, such as gate-tunable charged excitons [8–10] and biexcitons [11]. Optical excitation of these transition metal dichalcogenide monolayers with circularly polarized light has also been demonstrated as a method for directly accessing the valley degree of freedom associated with the degenerate K and K' valleys in the Brillouin zone [12–15]. Taking advantage of these light-matter interactions in monolayer TMDCs, researchers have demonstrated novel optoelectronic effects and have developed model optoelectronic devices [16–19]. However, despite the direct band-gap character of the TMDCs and the large oscillator strength of the excitonic transitions, quantum efficiencies for light emission remain relatively low. This suggests that fundamental aspects of the light emission process, critical for both basic studies of the material and emerging applications, remain to be understood.

Here, we present experimental evidence for the existence of an optically dark state in monolayer WSe₂. This state lies below the emissive band-edge (A) exciton by an energy of ∼30 meV. It strongly quenches the light emission from this material, at reduced temperature. These conclusions are based on detailed studies of the temperature-dependent photoluminescence (PL) and time-resolved photoluminescence (TR-PL). We extracted the thermalized population of the bright exciton species by careful analysis of its emission dynamics. The origin of the dark state can be understood in terms of the recently calculated spin splitting of the conduction band, the sign of which varies for different TMDC materials. For monolayer WX_2 (X = S, Se), electrons in the lowest conduction and highest valence band at K/K' points are predicted to have antiparallel spins, implying an optically dark state [20–24].

In our experiments, we investigated monolayers of WSe₂ (and, for comparison, of MoS₂) prepared by mechanical exfoliation of bulk crystals. For supported samples, we used a Si substrate with 285 nm SiO_2 overlayer, while suspended samples were exfoliated directly over etched holes in the same substrate. We also examined samples with variable charge density in a field-effect transistor structure. For this case, we applied a potential between the sample, connected by Ti/Au electrodes formed by e-beam lithography, and the Si substrate. We measured the photoluminescence spectra using a microscope coupled to a spectrometer with a CCD detector. For the TR-PL measurements, we utilized time-correlated single photon counting. A frequency-doubled mode-locked Ti:sapphire laser provided pulsed laser excitation of 100 fs duration and 400 nm wavelength at a repetition rate of 80 MHz. Further experimental details are provided in the Supplemental Material [25]. Throughout the experiment, low excitation fluence (< 1.2 μJ cm⁻²) was used to avoid such phenomena as exciton-exciton annihilation [38–40] and biexciton
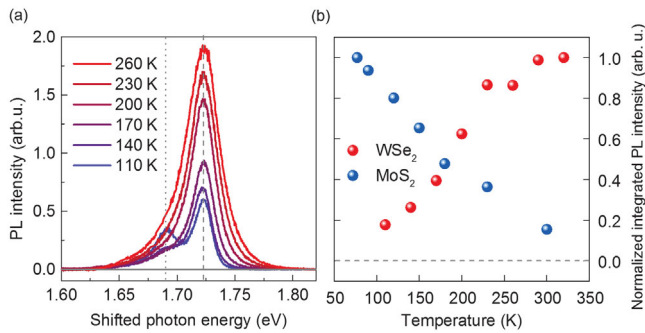
FIG. 1 (color).   (a) PL spectra of suspended monolayer WSe$_2$ at
different temperatures, excited by pulsed 400 nm radiation. To
facilitate comparison, the spectra at temperatures above 110 K
have been shifted horizontally to align the A exciton emission
feature (the dashed line). The spectrum at 260 K has, for example,
been blueshifted by 51 meV. (b) Comparison of temperature
dependence of the time-integrated PL intensity of WSe$_2$ and
MoS$_2$. In both cases, the maximum intensity is normalized to
unity. Excitation for the MoS$_2$ spectra was provided by a cw
532 nm laser.

formation [11], which are known to occur at high exciton
density.

We first present results of the temperature dependence
observed in time-integrated photoluminescence from
monolayer WSe$_2$. This measurement already indicates
the presence of a dark state in this system. For a high-
quality suspended monolayer, the PL spectrum is domi-
nated over the relevant temperature range by emission from
the neutral A (band-edge) exciton [Fig. 1(a)], with a weak
charged exciton emission feature emerging at low temper-
ature. Figure 1(b) displays the significant decrease in the A
exciton PL intensity observed when cooling from room
temperature down to 110 K. The same trend is observed
for a gated sample, with a doping level close to charge
neutrality (see the Supplemental Material [25]). The
decreasing PL with decreasing temperature suggests that
there is a lower-lying dark state that quenches emission
from the bright states. Since the trend in the PL is similar
for excitation both with near-resonant and higher-energy
photons, the possible temperature dependence of the trans-
fer efficiency from the initially excited state to the band-
edge exciton states appears to be insignificant under our
experimental conditions (see the Supplemental Material
[25]). Similar quenching of the PL intensity with decreas-
ing temperature has been observed in semiconducting
single-walled carbon nanotubes [41–43] and attributed to
theoretically predicted [44,45] lower-lying dark states. By
way of comparison, for a MoS$_2$ monolayer, precisely the
opposite trend in the temperature dependence of the PL is
observed: we find that the PL intensity of monolayer
MoS$_2$ increases with decreasing temperature, in agreement
with previous reports for monolayers MoS$_2$ and MoSe$_2$
[46–48]. This behavior can be understood on the basis of
improved exciton-photon coupling associated with a larger

fraction of the excitons lying within the radiative cone at
reduced temperature [49]. We note that changes in sample
temperature induce spectral shifts that slightly modify the
absorption of the exciting laser for the PL measurements.
Correcting for this effect does not, however, alter the trends
just described (see the Supplemental Material [25] for
details). A similar trend for the temperature dependence of
PL from WSe$_2$ was also recently reported [47,48].

The observed temperature dependence of the time-
integrated PL suggests the presence of a lower-lying dark
state in WSe$_2$. Such a state would be preferentially
populated at low temperature. It would thus reduce the
population in the higher-lying bright state and the corre-
sponding PL signal. While it is tempting to analyze the
variation in PL intensity directly in terms of the shift in the
equilibrium population from the bright to the dark state as a
function of temperature, such measurements are, in fact,
strongly influenced by other factors. In particular, in
addition to the expected variation of the radiative rate with
temperature alluded to above, competing nonradiative
decay channels could also exhibit a significant temperature
dependence. The temperature dependence of these rates
will directly affect the observed time-integrated PL inten-
sity. Furthermore, to extract energy differences between the
bright and dark states from the measured temperature
dependence of the PL also requires that the emission
process be governed by equilibrium populations in the
different states. This situation will not apply immediately
after the creation of excitation in the material.

Below, we make use of TR-PL to address these important
issues. Our approach is essentially to measure the initial
TR-PL signal, choosing a time after the excitons have
thermalized, but before the occurrence of significant
population decay through slower nonradiative channels.
This initial thermalized TR-PL signal is then directly
proportional to the total exciton population in the bright
state [50]. It only needs to be corrected for the radiative
decay rate, the temperature dependence of which can
be modeled by basic considerations of momentum
conservation.

The measured TR-PL traces from a suspended mono-
layer of WSe$_2$ are shown in Fig. 2(a) for selected temper-
atures. These data fit well to a rapid exponential decay
(< 10 ps), followed by a slower biexponential decay. The
underlying decay dynamics for each temperature, after
deconvolution of the instrument response function (IRF),
are presented in Fig. 2(b). In our data, we observe for all
temperatures one fast and one relatively slow relaxation
component for the A exciton emission. At room temper-
ature, the exciton relaxation time is long. With decreasing
temperature, while some excitons decay through slower
channels (60 ps–1 ns), there is an increasing portion
that relaxes on an ultrafast time scale (< 10 ps).
Eventually, at low temperature, the fast relaxation process
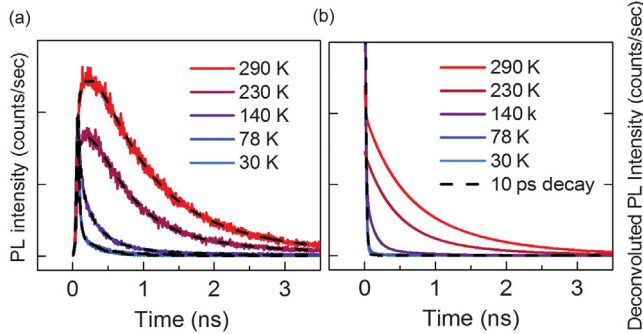dominates, in agreement with previous reports [40,51,52].

FIG. 2 (color).   TR-PL from a suspended monolayer of WSe$_2$.
(a) Time traces for A exciton emission measured at several
temperatures by time-correlated single photon counting. The
excitation is provided by a 400 nm pulsed laser with constant
pump power. The magnitudes of the curves can be compared
directly. The PL decay is fit (dashed lines) by the sum of three
exponential terms $I = [A_1 \exp(-t/\tau_1)]_{\text{fast}} + [A_2 \exp(-t/\tau_2) + A_3 \exp(-t/\tau_3)]_{\text{slow}}$ convolved with IRF. The fitted time traces
are indicated by black dashed lines. (b) The corresponding
deconvoluted PL time traces. The fast and slow decay compo-
nents can be readily identified at all temperatures.

The deconvoluted emission dynamics in Fig. 2(b) reveal a
clear distinction between the fast and slow decay
components.

We interpret the fast decay component in the TR-PL as
corresponding to an initial nonthermalized regime. For
our analysis, we consequently consider the longer-lived
response. The longer decay dynamics reflect both the
radiative lifetime and the nonradiative decay channels. To
further reduce the influence of these decay channels, the
thermalized emission intensity is extrapolated back to
$t = 0$, and $I_{\text{thermal}}(t = 0)$ is taken to be proportional to the
thermalized bright exciton population before any signifi-
cant decay has occurred. To convert the measured
emission signal to a quantity proportional to the total
exciton population in the bright state, we need to consider
the temperature variation of the radiative relaxation
rate. To conserve momentum, only excitons within the
radiative light cone can contribute to light emission.
In 2D systems, this leads to a radiative rate k_{rad}
varying inversely with temperature [49,53]. (See the
Supplemental Material [25] for additional discussion of
the exciton distribution.) Therefore, the initial thermal-
ized exciton population in the bright state scales as $N_X \propto I_{\text{thermal}}(t = 0)k_{\text{rad}}^{-1} \propto I_{\text{thermal}}(t = 0)T$.

We apply this method to extract the temperature variation
of the exciton population in the bright state for three
different monolayer WSe$_2$ samples, with varying doping
levels, defect densities, and prepared as suspended and
supported layers. The results are presented in Fig. 3(a). (See
the Supplemental Material [25] for a more detailed com-
parison.) Despite the different sample conditions, the
variation with temperature is consistent: with decreasing
temperature, the thermalized exciton population in the

bright state decreases sharply. At temperatures below
80 K, excitons mostly recombine through the fast (hot)
relaxation channel. There are extrinsic factors that might
contribute to a reduction of the A exciton population,
including the possible formation of trions and localized
defect or trap states at lower temperature. The estimated
densities of these species are, however, too low to account
for the observed quenching of the neutral exciton popula-
tion, as manifested in their almost identical trends of
thermal population in various samples. A more quantitative
approach is presented in the Supplemental Material [25].

We first analyze the bright state population in a simple
two-level model with a lower-lying dark state. In thermal
equilibrium, the bright state population follows the
Boltzman distribution:

$$N_X(T) = \frac{\exp(-\Delta/k_B T)}{\exp(-\Delta/k_B T) + 1} \text{const}, \qquad (1)$$

with Δ representing the bright-dark energy splitting. From
fitting Eq. (1) to the experimentally determined variation of
N_X with temperature, we obtain $\Delta = 30 \pm 5$ meV, as
shown in Fig. 3(a). In our analysis, we have used the
nominal sample temperature as representative of the exci-
ton temperature defining occupancy of the states. This
approach is justified by the fact that our TR-PL measure-
ments exclude the initial nonthermal regime (see the
Supplemental Material [25] for a discussion of the exciton
temperature). From the lack of a shift in the PL emission
peak with laser fluence and an estimation of the maximum
single pulse heating, we deduce a temperature rise of less
than 5 K (see the Supplemental Material [25] for estimation
details) for laser induced sample heating. We also note that
although intervalley dark excitons could recombine radi-
atively through a phonon-assisted process [54], we see no
evidence for the corresponding lower-energy emission
feature. Significant emission at lower photon energies is
present only at a sample temperature below 70 K, which we
attribute to defect-related emission. This suggests that the
phonon-assisted emission of the dark states is negligible
under our experimental conditions.

We now consider the physical origin of this dark state.
We first examine the character of the relevant electronic
bands in monolayer WSe$_2$ [20–24]. The direct optical
transitions occur at the K/K' point of the Brillouin zone,
where the valence band arises principally from the $d_{x^2-y^2}$
and d_{xy} orbitals of metal atoms. The valence band exhibits
strong spin orbit coupling and splits into two spin-polarized
bands separated by hundreds of meV. In the corresponding
simple theoretical picture, the conduction bands arise from
the d_{z^2} orbitals of metal atoms and, to leading order, no spin
splitting of the bands is expected. However, taking into
account the role of the less strongly coupled chalcogen
orbitals and of the higher-order couplings to other orbitals
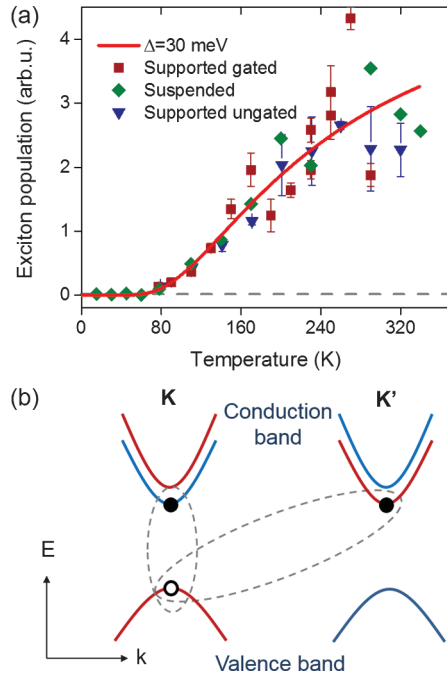of the metal atoms, it is predicted that the conduction band

FIG. 3 (color). (a) Temperature dependence of the thermalized exciton population, N_X, in the bright state for three different samples, compared to a fit (the red solid line) of a simple two-level model, with an activation energy of $\Delta = 30$ meV. The red symbols correspond to a gated sample tuned to close to charge neutrality, the green symbols to a suspended sample, and the blue triangle to a supported sample on a SiO_2/Si substrate. Both ungated samples are unintentionally n doped. The error bars reflect the inhomogeneity over different spatial regions of large supported samples. (b) A schematic representation of the upper valence and conduction band structure predicted for monolayer WSe_2, with blue and red corresponding to the two spin states of electrons. The conduction band splitting is responsible for the dark exciton states. Shown by dotted lines are the lowest energy excitons: the intravalley dark excitons, i.e., $|K_{e\uparrow}K_{h\uparrow}\rangle$ and $|K'_{e\downarrow}K'_{h\downarrow}\rangle$, and the intervalley dark excitons, i.e., $|K_{e\uparrow}K'_{h\downarrow}\rangle$ and $|K'_{e\uparrow}K_{h\uparrow}\rangle$.

will exhibit a spin splitting of tens of meV. The sign of this conduction band splitting varies among the different TMDC materials due to the competition between these two contributions. Specifically, for WX_2 ($X = S$, Se), electrons in the lower conduction band are expected to have spin polarization opposite to those in the upper valence band; in contrast, for MoX_2 ($X = S$, Se), electrons in the lower conduction band are expected to have spin polarization that matches that in the upper valence band [20–24].

We now examine the energies of the different possible excitonic states, taking into account the spin and valley degrees of freedom at the K/K' points. Because of the large spin splitting in the valence band, for the A exciton emission, we need only to consider photoexcited holes as residing in the upper valence band. For the photoexcited electrons, however, there are four possible states (two valleys and two

spins). We thus have a total of eight different species of excitons. Among them, there are two bright excitons—i.e., the singletlike intravalley excitons—and six dark excitons—i.e., the tripletlike intravalley excitons and all intervalley excitons. In our discussion, we first neglect e-h exchange interactions (a related modification will be discussed later). The energies of bright and dark excitons are then determined by the band splitting [55]. For WSe_2, with the conduction band ordering described above, the tripletlike intravalley excitons and the singletlike intervalley excitons are degenerate and have the lowest energy, as depicted schematically in Fig. 3(b). The tripletlike intervalley excitons have a higher energy, which is the same as that of the bright excitons. In thermal equilibrium, the fraction of the total exciton population in bright states is given by $[\exp(-\Delta/k_BT)/2\exp(-\Delta/k_BT) + 2]$. This expression yields the same characteristic temperature variation as the simple two-level model introduced above and $\Delta = 30 \pm 5$ meV. A correction to this treatment arises from the presence of charged excitons. We consider this factor in a more complete analysis in the Supplemental Material [25], but, for the most heavily doped samples in our study, a similar level splitting of ~ 28 meV is inferred.

With respect to the mechanism leading to equilibrium between these different states, we are concerned with the behavior on a time scale longer than ~ 60 ps in our measurement. Bright states can relax to dark states by intervalley electron scattering or by spin flip of the electron. We expect that the spin-conserving intervalley scattering will be efficient in view of the availability of appropriate phonons for the process [56] and that thermal equilibrium will be established between these states on the time scale relevant for optical emission. Indeed, fast intervalley scattering (on a time scale of picoseconds) has been inferred from recent time-resolved spectroscopy measurements [57,58]. In our measurements, the excitation conditions (linearly polarized light) do not favor one valley over the other. Within the single particle picture, the occupation of all four conduction bands will be governed by equilibrium populations based on rapid intervalley scattering by spin-conserving processes.

In our discussion above, we neglected the influence of e-h exchange interactions. These interactions would lead to a more complex spectrum of states. In particular, the long-range component of exchange interaction is expected to increase the energy of intravalley excitons with a singletlike configuration compared to that of tripletlike excitons [59]. This trend has been experimentally verified in III-V quantum well systems, in which both long-range and short-range components contribute [60,61]. The exchange interaction would affect intervalley excitons in a similar way, but it is expected to be weaker [15]. Therefore, including the exchange interactions will not change the ordering of bright and dark excitons for WSe_2, but the splitting will deviate from the spin splitting of the conduction band, and the energies of the intravalley and intervalley dark excitons will

become nondegenerate. Within this picture, we should then interpret the inferred Δ as reflecting the conduction band splitting, modified by an averaged intra- and intervalley exchange interaction. For the case of monolayer MoS_2, where the predicted conduction band splitting is only 2–3 meV and of opposite sign compared to exchange splitting, the role of exchange interactions may be more critical in defining the ordering of dark and bright states.

The presence of the dark states identified in this Letter leads to a reduction in light emission for the complex of band-edge excitons. Population in the dark state must be thermally activated for radiative emission. At reduced temperatures, thermal activation from the dark state can be strongly suppressed. In this case, the lifetime of excitons in the dark state, in the absence of radiative decay channels, can become very long. This presents an opportunity to investigate new many-body effects, such as Bose-Einstein condensation, without the complication of rapid radiative channels [62,63].

---

[*]Corresponding author.
tony.heinz@stanford.edu

[1] K. F. Mak, C. Lee, J. Hone, J. Shan, and T. F. Heinz, Phys. Rev. Lett. **105**, 136805 (2010).

[2] A. Splendiani, L. Sun, Y. Zhang, T. Li, J. Kim, C.-Y. Chim, G. Galli, and F. Wang, Nano Lett. **10**, 1271 (2010).

[3] A. Chernikov, T. C. Berkelbach, H. M. Hill, A. Rigosi, Y. Li, O. B. Aslan, D. R. Reichman, M. S. Hybertsen, and T. F. Heinz, Phys. Rev. Lett. **113**, 076802 (2014).

[4] Z. Ye, T. Cao, K. O'Brien, H. Zhu, X. Yin, Y. Wang, S. G. Louie, and X. Zhang, Nature (London) **513**, 214 (2014).

[5] K. He, N. Kumar, L. Zhao, Z. Wang, K. F. Mak, H. Zhao, and J. Shan, Phys. Rev. Lett. **113**, 026803 (2014).

[6] M. M. Ugeda, A. J. Bradley, S.-F. Shi, H. Felipe, Y. Zhang, D. Y. Qiu, W. Ruan, S.-K. Mo, Z. Hussain, Z.-X. Shen et al., Nat. Mater. **13**, 1091 (2014).

[7] B. Zhu, X. Chen, and X. Cui, Sci. Rep. **5**, 9218 (2015).

[8] K. F. Mak, K. He, C. Lee, G. H. Lee, J. Hone, T. F. Heinz, and J. Shan, Nat. Mater. **12**, 207 (2013).

[9] J. S. Ross, S. Wu, H. Yu, N. J. Ghimire, A. M. Jones, G. Aivazian, J. Yan, D. G. Mandrus, D. Xiao, W. Yao et al., Nat. Commun. **4**, 1474 (2013).

[10] A. A. Mitioglu, P. Plochocka, J. N. Jadczak, W. Escoffier, G. L. J. A. Rikken, L. Kulyuk, and D. K. Maude, Phys. Rev. B **88**, 245403 (2013).

[11] Y. You, X.-X. Zhang, T. C. Berkelbach, M. S. Hybertsen, D. R. Reichman, and T. F. Heinz, Nat. Phys. **11**, 477 (2015).

[12] K. F. Mak, K. He, J. Shan, and T. F. Heinz, Nat. Nanotechnol. **7**, 494 (2012).

[13] H. Zeng, J. Dai, W. Yao, D. Xiao, and X. Cui, Nat. Nanotechnol. **7**, 490 (2012).

[14] T. Cao, G. Wang, W. Han, H. Ye, C. Zhu, J. Shi, Q. Niu, P. Tan, E. Wang, B. Liu et al., Nat. Commun. **3**, 887 (2012).

[15] A. M. Jones, H. Yu, N. J. Ghimire, S. Wu, G. Aivazian, J. S. Ross, B. Zhao, J. Yan, D. G. Mandrus, D. Xiao et al., Nat. Nanotechnol. **8**, 634 (2013).

[16] L. Britnell, R. Ribeiro, A. Eckmann, R. Jalil, B. Belle, A. Mishchenko, Y.-J. Kim, R. Gorbachev, T. Georgiou, S. Morozov et al., Science **340**, 1311 (2013).

[17] K. F. Mak, K. L. McGill, J. Park, and P. L. McEuen, Science **344**, 1489 (2014).

[18] Y. Zhang, T. Oka, R. Suzuki, J. Ye, and Y. Iwasa, Science **344**, 725 (2014).

[19] R. Cheng, D. Li, H. Zhou, C. Wang, A. Yin, S. Jiang, Y. Liu, Y. Chen, Y. Huang, and X. Duan, Nano Lett. **14**, 5590 (2014).

[20] G.-B. Liu, W.-Y. Shan, Y. Yao, W. Yao, and D. Xiao, Phys. Rev. B **88**, 085433 (2013).

[21] K. Kośmider and J. Fernández-Rossier, Phys. Rev. B **87**, 075451 (2013).

[22] K. Kośmider, J. W. González, and J. Fernández-Rossier, Phys. Rev. B **88**, 245436 (2013).

[23] A. Kormányos, V. Zólyomi, N. D. Drummond, and G. Burkard, Phys. Rev. X **4**, 011034 (2014).

[24] A. Kormányos, G. Burkard, M. Gmitra, J. Fabian, V. Zólyomi, N. D. Drummond, and V. Falko, 2D Mater. **2**, 022001 (2015).

[25] See Supplemental Material at http://link.aps.org/supplemental/10.1103/PhysRevLett.115.257403, which includes Refs. [26–37], for experimental methods, discussion of heating effects, consideration of trions defect-related states, and the temperature dependency of exciton generation efficiency.

[26] J.-Y. Kim, S.-M. Choi, W.-S. Seo, and W.-S. Cho, Bull. Korean Chem. Soc. **31**, 3225 (2010).

[27] B. N. Murdin, W. Heiss, C. J. G. M. Langerak, S.-C. Lee, I. Galbraith, G. Strasser, E. Gornik, M. Helm, and C. R. Pidgeon, Phys. Rev. B **55**, 5171 (1997).

[28] B. Murdin, G. Knippels, A. Van der Meer, C. Pidgeon, C. Langerak, M. Helm, W. Heiss, K. Unterrainer, E. Gornik, K. Geerinck et al., Semicond. Sci. Technol. **9**, 1554 (1994).

[29] K. Kaasbjerg, K. S. Thygesen, and K. W. Jacobsen, Phys. Rev. B **85**, 115317 (2012).

[30] N. Balkan, H. Çelik, A. J. Vickers, and M. Cankurtaran, Phys. Rev. B **52**, 17210 (1995).

[31] H. Yoon, D. Wake, and J. Wolfe, Phys. Rev. B **54**, 2763 (1996).

[32] C. Pöllmann, P. Steinleitner, U. Leierseder, P. Nagler, G. Plechinger, M. Porer, R. Bratschitsch, C. Schüller, T. Korn, and R. Huber, Nat. Mater. **14**, 889 (2015).

[33] T. Damen, J. Shah, D. Oberli, D. Chemla, J. Cunningham, and J. Kuo, Phys. Rev. B **42**, 7434 (1990).

[34] C. F. Klingshirn, Semiconductor Optics (Springer Science +Business Media, New York, 2012).

[35] B. Arnaudov, T. Paskova, P. Paskov, B. Magnusson, E. Valcheva, B. Monemar, H. Lu, W. Schaff, H. Amano, and I. Akasaki, Phys. Rev. B **69**, 115216 (2004).

[36] Y. Li, A. Chernikov, X. Zhang, A. Rigosi, H. M. Hill, A. M. van der Zande, D. A. Chenet, E.-M. Shih, J. Hone, and T. F. Heinz, Phys. Rev. B **90**, 205422 (2014).

[37] D. Kozawa, R. Kumar, A. Carvalho, K. K. Amara, W. Zhao, S. Wang, M. Toh, R. M. Ribeiro, A. C. Neto, K. Matsuda *et al.*, Nat. Commun. **5**, 4543 (2014).

[38] D. Sun, Y. Rao, G. A. Reider, G. Chen, Y. You, L. Brézin, A. R. Harutyunyan, and T. F. Heinz, Nano Lett. **14**, 5625 (2014).

[39] N. Kumar, Q. Cui, F. Ceballos, D. He, Y. Wang, and H. Zhao, Phys. Rev. B **89**, 125427 (2014).

[40] S. Mouri, Y. Miyauchi, M. Toh, W. Zhao, G. Eda, and K. Matsuda, Phys. Rev. B **90**, 155449 (2014).

[41] I. B. Mortimer and R. J. Nicholas, Phys. Rev. Lett. **98**, 027404 (2007).

[42] S. Berger, C. Voisin, G. Cassabois, C. Delalande, P. Roussignol, and X. Marie, Nano Lett. **7**, 398 (2007).

[43] J. Shaver and J. Kono, Laser Photonics Rev. **1**, 260 (2007).

[44] C. D. Spataru, S. Ismail-Beigi, R. B. Capaz, and S. G. Louie, Phys. Rev. Lett. **95**, 247402 (2005).

[45] V. Perebeinos, J. Tersoff, and P. Avouris, Nano Lett. **5**, 2495 (2005).

[46] S. Tongay, J. Zhou, C. Ataca, K. Lo, T. S. Matthews, J. Li, J. C. Grossman, and J. Wu, Nano Lett. **12**, 5576 (2012).

[47] A. Arora, M. Koperski, K. Nogajewski, J. Marcus, C. Faugeras, and M. Potemski, Nanoscale **7**, 10421 (2015).

[48] G. Wang, C. Robert, A. Suslu, B. Chen, S. Yang, S. Alamdari, I. C. Gerber, T. Amand, X. Marie, S. Tongay *et al.*, arXiv:1506.08114.

[49] L. C. Andreani, F. Tassone, and F. Bassani, Solid State Commun. **77**, 641 (1991).

[50] The total exciton population includes both excitons in the light cone, and the large-momentum excitons outside the light cone. The temperature-dependent radiative rate accounts for the varying ratio of excitons inside and outside the light cone.

[51] G. Wang, L. Bouet, D. Lagarde, M. Vidal, A. Balocchi, T. Amand, X. Marie, and B. Urbaszek, Phys. Rev. B **90**, 075413 (2014).

[52] T. Yan, X. Qiao, X. Liu, P. Tan, and X. Zhang, Appl. Phys. Lett. **105**, 101901 (2014).

[53] J. Feldmann, G. Peter, E. O. Göbel, P. Dawson, K. Moore, C. Foxon, and R. J. Elliott, Phys. Rev. Lett. **59**, 2337 (1987).

[54] G. Wang, L. Bouet, M. M. Glazov, T. Amand, E. L. Ivchenko, E. Palleau, X. Marie, and B. Urbaszek, 2D Mater. **2**, 034002 (2015).

[55] Here, we neglect the possible difference in the binding energy of different excitonic species present within an effective mass model.

[56] H. Terrones, E. Del Corro, S. Feng, J. Poumirol, D. Rhodes, D. Smirnov, N. Pradhan, Z. Lin, M. Nguyen, A. Elias *et al.*, Sci. Rep. **4**, 4215 (2014).

[57] Q. Wang, S. Ge, X. Li, J. Qiu, Y. Ji, J. Feng, and D. Sun, ACS Nano **7**, 11087 (2013).

[58] C. R. Zhu, K. Zhang, M. Glazov, B. Urbaszek, T. Amand, Z. W. Ji, B. L. Liu, and X. Marie, Phys. Rev. B **90**, 161302 (2014).

[59] M. Rohlfing and S. G. Louie, Phys. Rev. B **62**, 4927 (2000).

[60] H. W. van Kesteren, E. C. Cosman, W. A. J. A. van der Poel, and C. T. Foxon, Phys. Rev. B **41**, 5283 (1990).

[61] S. Glasberg, H. Shtrikman, I. Bar-Joseph, and P. C. Klipstein, Phys. Rev. B **60**, R16295 (1999).

[62] J. I. Jang and J. P. Wolfe, Phys. Rev. B **74**, 045211 (2006).

[63] D. Snoke and G. Kavoulakis, Rep. Prog. Phys. **77**, 116501 (2014).